 SDHM, vol.13, no.2, pp.205-225, 2019

# Load Test and Fatigue Life Evaluation for Welded Details in Taizhou Yangtze River Bridge

**Meiling Zhuang[1, 2], Changqing Miao[1, 2, *] and Rongfeng Chen[1, 2]**

**Abstract:** To study the fatigue performance of welded details in the orthotropic steel decks, the steel box girder for Taizhou Yangtze River Bridge is taken as the research object. Based on the field monitoring data obtained from the load test, the stress response test of the orthotropic steel box girder under wheel loads is performed and the correctness of the vehicle test data obtained from the field monitoring data also have been verified by the numerical results of the finite element model. Based on the Miner linear cumulative damage theory, the S-N curve of the Eurocode3 specification is referenced, and the fatigue life calculation formula of the welded details is determined according to the actual structural features. The fatigue life evaluation of the four typical welded details is obtained. The results indicate that: The load test data is compared and verified by the numerical result of finite element model. The local effect of stress distribution is remarkable. The stress measurement points on the four typical welded details are mainly based on low amplitude stress cycles. Most of the stress ranges are 2-10 MPa, among which the stress range of the welded details at the U-rib butt joint is larger. The fatigue life of welded details in the 14 mm thick top plate is smaller than that of the 16 mm thick top plate corresponding to the fatigue life of the welded details. The rib-to-rib butt welded joints and the openings of the diaphragms were prone to fatigue failure. Among them, the welding details of the 14 mm thick U-rib butt joints first appeared fatigue failure. The arrangement of the diaphragm can effectively increase the fatigue life of the top-U rib weld and improve the fatigue performance at this detail.

**Keywords:** Orthotropic steel bridge decks, welded details, fatigue stress spectra, fatigue life.

## 1 Introduction

The orthotropic steel box girders as the main structure of the stiffening girder have been widely used for long span suspension highway bridges due to their overall light weight, convenient construction and high bearing capacity [Fisher and Roy (2011)]. A typical modern orthotropic deck usually consists of a thin steel deck plate stiffened by longitudinal ribs and transverse diaphragms. Closed longitudinal ribs are prevalently used for lighter weight, fewer welds and higher torsional and flexural stiffness [Kozy and

[1] Key Laboratory of Concrete and Prestressed Concrete Structure of Ministry of Education，Southeast University, Nanjing, 210096, China.

[2] School of Civil Engineering, Southeast University, Nanjing, 210096, China.

[*] Corresponding Author: Changqing Miao. Email: chqmiao@seu.edu.cn.

Connor (2010); Sim and Uang (2012). The orthotropic steel box girder suffers from complicated forces, and has many types of joints and structural details. The steel deck has a large flexibility, which is susceptibe to fatigue cracking under high cyclic stresses by wheel loads [Fu, Zhang, Wang et al. (2014); Ju and Tateishi (2014)], which are really hard to repair. In recent years, the fatigue failure of orthotropic steel bridge deck has become increasingly prominent, which has been a hot spot [Zhu, Li, Tian et al. (2017); Zhang, Cui, Bu et al. (2015); Zhang, Bu and Qiao (2017)].

The study of fatigue performance of orthotropic bridge decks abroad is relatively early. The design specifications have been compiled, such as BS5400 in the United Kingdom [BS5400 (1980)], AASHTO in the United States, see [ASHTO (2010); ASHTO (2012); AISC (2010)], and Eurocode3 in Europe [EC3(2004)]]. In recent decades, the application of orthotropic steel bridge decks in China's large-span highway bridges has developed rapidly. However, the fatigue research and design specification lags behind the construction of bridges, and fatigue design is usually performed with reference to foreign regulations [Gurney (2006); Song, Ding, Wan et al. (2013); Deng, Ding and Li (2013); Zeng, Zhang, Cui et al. (2015); Liu, Xiao, Lu, et al. (2016); Chang and Bae (2014); Yang and Zhou (2017); Guo and Chen (2013); Miao and Shi (2013)].

For the fatigue problem of orthotropic steel box girder, the fatigue properties of steel box girder welded details under wheel loads are widely studied through experiments and linear fatigue accumulation methods. Tang et al. [Tang, Huang, Liu et al. (2014)] studied the fatigue stress of several typical details in the orthotropic steel deck in China through the full scale model fatigue test of orthotropic steel deck. Ji et al. [Ji, Liu, Chen et al. (2013)] evaluated the fatigue durability of the root-deck fatigue over diaphragm in orthotropic bridge deck by using the finite element (FEM) model. Zhang et al. [Zhang, Cui, Bu et al. (2014)] made experiment and studied the fatigue vulnerable parts of 5 important orthotropic steel decks by full scale model, and established a fatigue damage crack propagation simulation method based on theoretical model and elastic-plastic fracture mechanics. Ya et al. [Ya, Yamada and Shikawa (2011)] reported fatigue test results of 300-mm-wide specimens with three details: 80% partial joint penetration (80%PJP), weld melt-through (WMT). Liu et al. [Liu, Zhang, Zhang et al. (2016)] took Hong Kong-Zhuhai-Macao Bridge as an example, and established the numerical simulation method for crack propagation of U-rib butt welds in orthotropic steel deck based on linear elastic fracture theory. The effectiveness and feasibility of numerical simulation method is verified by model test.

However, the conventional fatigue evaluation is simulated under the condition of investigating vehicle loads. There are various assumptions by this method which cannot truly reflect the actual stress of the bridge. The most reliable and effective method is to directly collect the fatigue strain data of the key components of the steel box orthotropic steel deck under loads and obtain real fatigue stress spectrum method, thus the fatigue life of the orthotropic steel deck can be evaluated in a reliable way [Deng, Ding and Li (2013)]. Song et al. [Song, Ding, Wang et al. (2013)] studied the correlation between the ambient temperature and the two key welded details under traffic loads, based on the results of monitoring long-term effects of fatigue Runyang Bridge. The results show that

the number of stress cycles of the two types of welded details is linearly related to the vehicle flow and not to the ambient temperature. Deng et al. [Deng, Ding and Li (2013)] took long-term strain monitoring data of Runyang Bridge steel box girder as the research object, and studied the massive strain monitoring data analysis and fatigue assessment methods. Research suggested that the average strain caused by the temperature variation of the welded details is very small. Therefore, fatigue assessment of welded details can be made without considering the effects of temperature changes. Many weld joints in orthotropic deck are fatigue-sensitive parts. Many investigations and studies have shown that the following parts of the fatigue disease accounts for more than 90% of the total diseases, which is the fatigue vulnerable parts of the steel box orthotropic steel bridge deck [Gurney (2006); Song, Ding, Wang et al. (2013); Deng, Ding and Li (2013)]: ① U-rib ribbed slot; ② Diaphragm and U-rib welds; ③ Steel box girder deck and U-rib; ④ U-rib butt joint. At present, the fatigue life of the above four types of key weld details is less studied based on the real-bridge load test.

In order to improve the anti-fatigue design of steel box orthotropic steel bridge decks, this article focuses on t the above 4 key welds of Taizhou Yangtze River Bridge, and evaluates the fatigue performance of each welded detail under 14 mm and 16 mm thick decks combined with the load test of Taizhou Yangtze River Bridge.

## 2 Fatigue stress monitoring of Taizhou Yangtze River Bridge under vehicle loads

### *2.1 Engineering background*

The profile of Taizhou Yangtze River Bridge is shown in Fig. 1. Taizhou Yangtze River Bridge lies between Taizhou, Zhenjiang and Changzhou City in Jiangsu Province. The total length of Taizhou Bridge is 62.088 km. The whole line is designed by freeway codes with six lanes in two directions. The main bridge crossing the Yangtze River is a continuous three-pylon two-span suspension bridge with the main span of 1080 m. It is open to traffic in 2012.

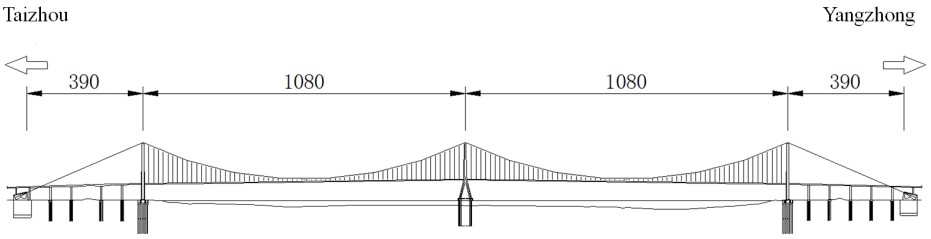


**Figure1:** Profile of Taizhou Yangtze River Bridge (dimensions in m)

The typical box-girder segment of Taizhou Yangtze River Bridge is shown in Fig. 2. The girder, including wind fairing, is 39.1 mm×3.5 mm, the roof width is 36.7 m, the floor width is 21.25 m, the transverse spacing of straight webs is 33.2 m, the spacing of transverse diaphragm is 3.2 m, and the spacing of U-ribs is 600 mm. The outside of the middle lane roof within the range of 6 m is 16 mm thick, and the U-rib is 8 mm thick, the remaining area roof is 14 mm thick, and the U-rib is 6 mm thick. The main structure of the box girder is made from Q345-D steel. The main parameters are roof thickness ($t_d$), U-rib

thickness ($t$), U-rib height ($H$) and U-rib opening size ($a$), respectively. The values of the parameters are as following: On the ordinary lane, $t_{d1}$=14 mm, $t_1$=6 mm, $H_1$=280 mm, $a_1$=300 mm. On the heavy truck lane, $t_{d2}$=16 mm, $t_2$=8 mm, $H_2$=280 mm, $a_2$=300.2 mm.

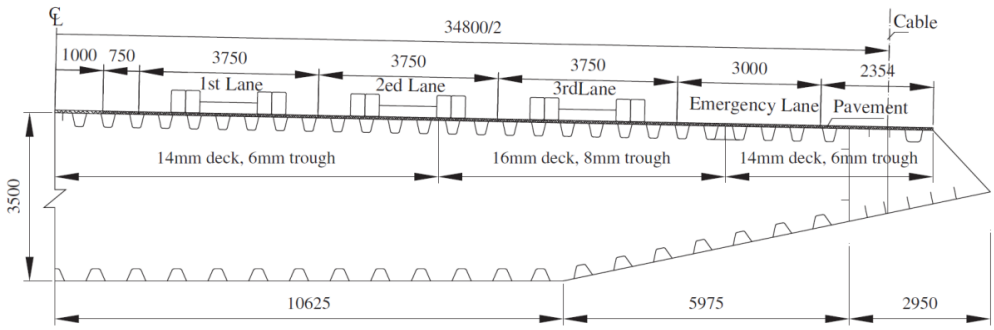


**Figure 2:** Local cross section diagram of the typical box-girder segment

### *2.3 Fatigue stress monitoring*

According to the load test of Taizhou Yangtze River Bridge, the stress distribution test and stress response test of welded details in the steel box girder were performed. The Five test sections in the N26 hosting girder section (two standard box-girder sections) near the L/4 side was selected in this load test. The strain monitoring was performed on the welding details of the rib-to-deck plate, U-rib butt joint, deck plate-to- rib-to-diaphragm and diaphragm plate opening.

Because of the different thicknesses of the deck and U-rib, the fatigue properties of the welded details in different deck thicknesses were compared and studied. The measurement points were symmetrically arranged on the 14 mm and 16 mm thick deck. Among them, the top plate-to-rib welded detail was arranged with one-way and two-way strain gages to monitor strains of the top plate-to- rib in both transverse and longitudinal directions. One-way strain gauges in longitudinal direction were arranged on U-rib butt joint. Due to the complicated stress distribution of the welding details at the diaphragm, in the position of the diaphragm, strain flowers were arranged on the diaphragm, and two kinds of strain gauges are arranged on the top plate, one-way and two-way. The location and number of the girder sections and measuring points in the steel box girder were located are shown in Fig. 3 (“S” represents Section, “L” represents Location). The details of the location of the measuring points were shown in Tab. 1. In Fig. 3 and Tab. 1, 1-1/1-2 show that the strain gauge is bidirectional point, along the bridge of 1-1, 1-2 for the transverse direction; 3-9/3-10/3-11 indicates that this position is a strained flower, and the cross-bridge strain is measured from 3-9, the oblique 45-degree strain can be obtained from 3-10, and the vertical-bridge strain from 3-11.

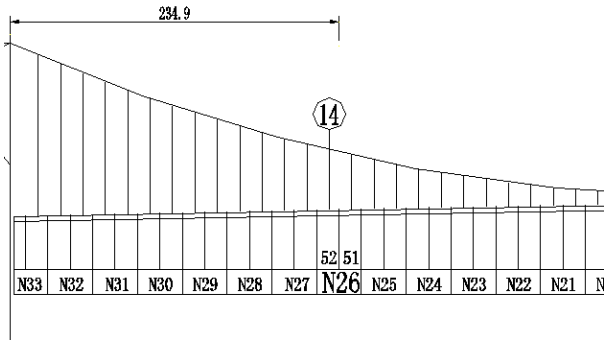


(a) The measuring steel box-girder Section

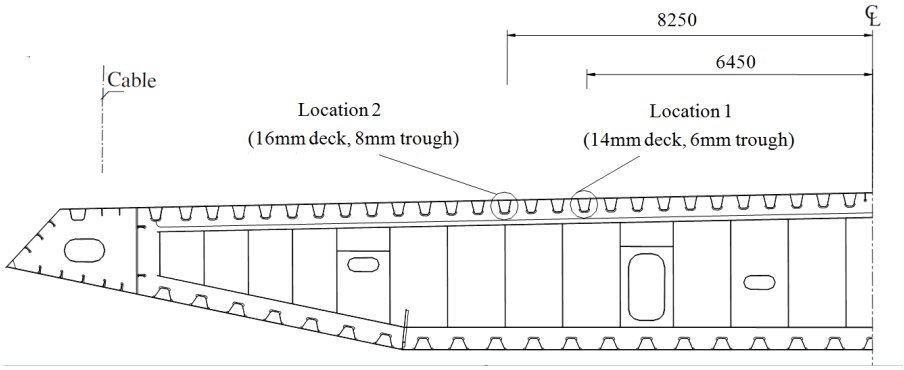


(b) Cross section of the steel box- girder (dimensions in mm)

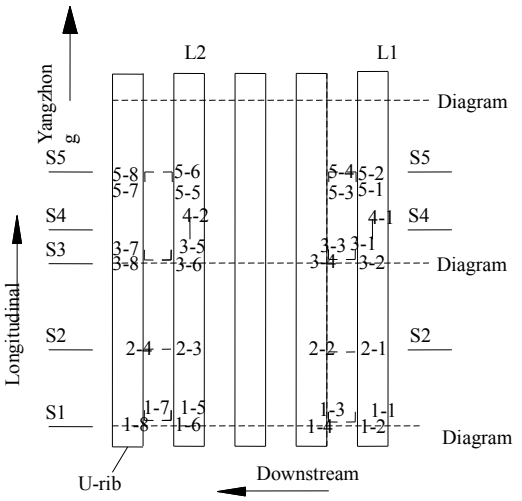


(c) Welded details

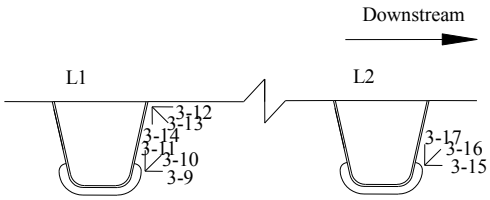


(d) Diagram on Section 3

**Figure 3:** Measuring points and strain gauges layout in the steel box-girders

**Table 1:** Detail types of the measuring point location

| Sections | Deck thickness (mm) | Measuring point location | Detail category |
|---|---|---|---|
| Section 1 | 14 | 1-1/1-2 | Deck plate-to-rib |
| | | 1-3/1-4 | Deck plate-to-rib |
| | 16 | 1-5/1-6 | Deck plate-to-rib |
| | | 1-7/1-8 | Deck plate-to-rib |
| Section 2 | 14 | 2-1 | Deck plate-to-rib |
| | | 2-2 | Deck plate-to-rib |
| | 16 | 2-3 | Deck plate-to-rib |
| | | 2-4 | Deck plate-to-rib |
| Section 3 | 14 | 3-1/3-2 | Deck plate-to-rib |
| | | 3-3/3-4 | Deck plate-to-rib |
| | | 3-9/10/11 | diaphragm plate opening |
| | | 3-12/13/14 | Deck plate-to-rib-to-diaphragm |
| | 16 | 3-5/3-6 | Deck-U-rib |
| | | 3-7/3-8 | Deck-U-rib |
| | | 3-15/16/17 | diaphragm plate opening |
| Section 4 | 14 | 4-1 | U-rib butt joint |
| | 16 | 4-2 | U-rib butt joint |
| Section 5 | 14 | 5-1/5-2 | Deck plate-to-rib |
| | | 5-3/5-4 | Deck plate-to-rib |
| | 16 | 5-5/5-6 | Deck plate-to-rib |
| | | 5-7/5-8 | Deck plate-to-rib |

(a) Diaphragm plates

(b) Deck plate

(c) U-rib butt joint

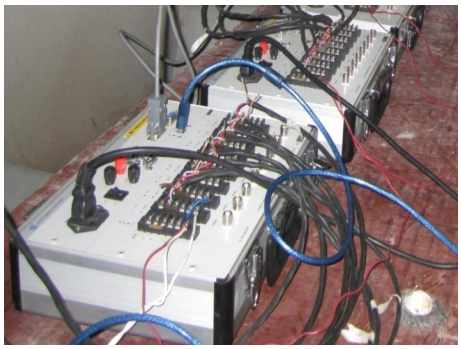

(d) Instrument field connections

**Figure 4:** The site layout of measuring points and the instrument connections

The site layout of measuring points and the instrument connection are shown in Fig. 4. Donghua DH 3817 and TEST 3827 dynamic and static signal test instruments are used to collect data. Each instrument has 8 test channels, and the instruments are connected in series. 1/4 bridge mode is selected as the strain gage connection mode. The temperature is compensated. The sampling frequency is 100 Hz.

The trial-loaded vehicle uses a three-axle truck with a total weight of 300 kN. The weight of the front axle is 60 kN. The center and rear axles are 120 kN. The specific vehicle parameters are shown in Fig. 5.

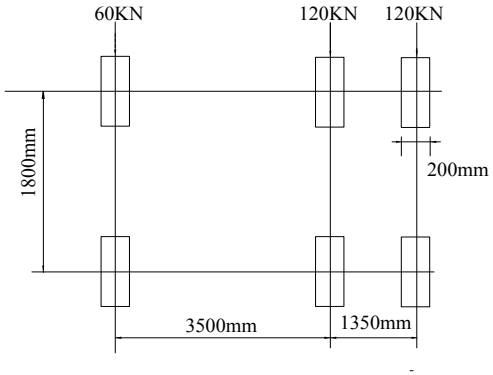


**Figure 5:** A vehicle load diaphragm

## 3 Finite element analysis

### *3.1 Finite element modeling*

The real bridge test datum is compared and verified by the numerical results of finite element model. The model of the box-girder segment of Taizhou Yangtze River Bridge under load test is established by ANSYS based on APDL (ANSYS Parametric Design Language). The structure size in the finite element model is consistent with the real bridge. Because of the thin wall structure of the flat steel box girder, a four-node plate/shell element in the ANSYS cell library called the shell63 with each node having six degrees of freedom is used in the finite element model. To accurately reflect the

structural deformation, stress conditions and detailed effects (e.g., top plate longitudinal ribbed stiffener) in the temperature loads, such a structure is detailed and discretized according to the actual composition of the top plates, sloping webs, transverse diaphragms and U-ribs of the steel box girder. The plate/shell element thickness of each site is the actual thickness of the steel plate at such a site. Steel has a thermal expansion coefficient of $1.2\times10^{-5}$ W $m^{-2}$ $^{o}C^{-1}$, elasticity modulus of $2.1\times10^{-5}$ MPa and Poisson's ratio ($v$) of 0.3. The constraints along the bridge of the finite element model are applied to the cross section of the girder both ends to meet the actual boundary conditions. The finite element model of the box-girder is shown in Fig. 6.

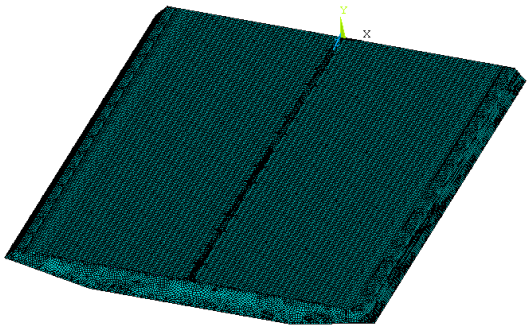

**Figure 6:** The finite element model

The load test of Taizhou Yangtze River Bridge had two parts: a vehicle test and a fleet test. In the finite element model, a fatigue vehicle in Fig. 5 is applied and the stress results were used to verify the correctness of a vehicle test data. The loading cases of finite element model are shown in Fig. 7 (taking Location 2 as an example). In the fleet test, the team had a total of 13 vehicles, each with a 20-m spacing along the bridge, with a vehicle speed of 40 km/h and driving at the same time. The lateral position of the wheels was the same as that of a vehicle test in loading case 3.

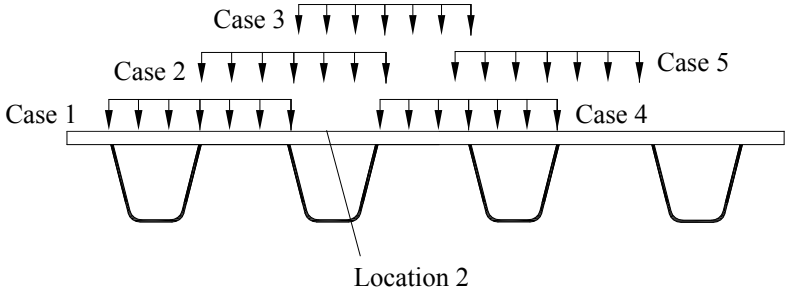


**Figure 7:** Loading cases

### *3.2 Stress analysis of welded details under a vehicle test*

There are many measuring points in this test. The same test item will have different sections for comparison, and the same law is obtained in the analysis. In order to save

space, this article lists two typical measuring points. The stress distribution of measuring points 2-3 (Deck plate-to-rib welded detail) can be seen in Fig. 8. The stress distribution of measuring points 4-2 (U-rib butt joint) can be seen in Fig. 9.

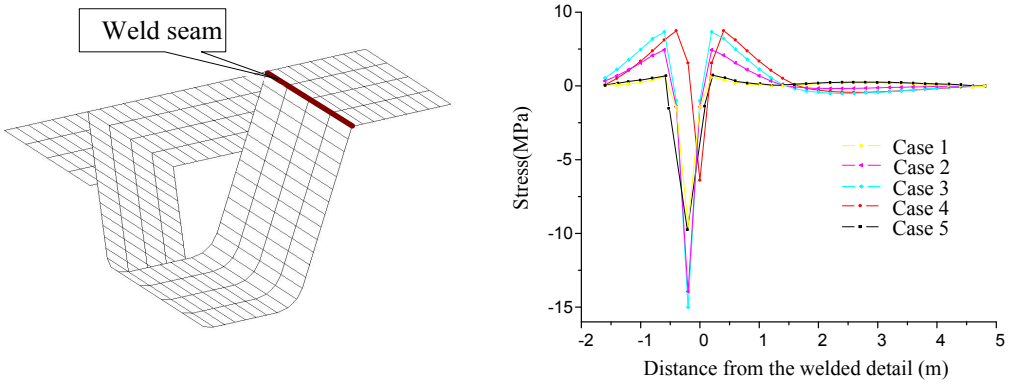


(a) Deck plate-to-rib weled detail (b) The stress lines

**Figure 8:** The finite element model results on measuring point 2-3

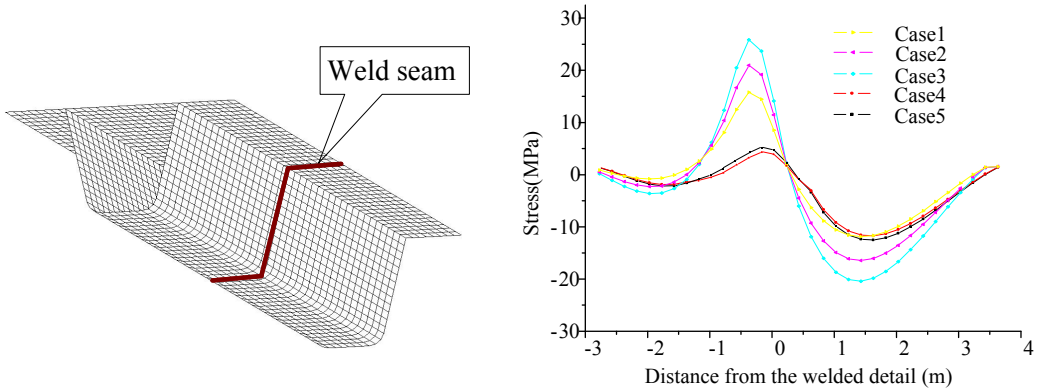


(a) U-rib butt joint (b) The stress lines

**Figure 9:** The finite element model results on measuring point 4-2

It can be seen from Fig. 8 that: In loading case 3, the wheel load center coincides with the measuring point 2-3; and the stress response at point 2-3 is the most obvious. In loading cases 2 and 4, the wheel center is closer to point 2-3. The stress response trend of the measuring point in loading cases 2 and 4 are relatively close with that in loading case 3. But the stress in loading cases 2 and 4 is smaller than that in loading case 3. In loading cases 1 and 5, the center of the wheel is far from the measuring point; and the stress response is smallest and the trend is not obvious. The local effect of the top deck plate stress distribution is remarkable under the wheel loads. The length of lateral stress lines

of the top deck plate is short. The stress distribution of the top deck plate is affected by the longitudinal ribs.

It is found from Fig. 9 that the stress distribution characteristics of U-rib butt joint is the same as that of the deck plate-to-rib welded detail under the wheel loads. The stress response of the longitudinal rib has strong local characteristics. The length of the lateral stress influence line is shorter. The stress distribution of U-rib butt joint is affected by the longitudinal ribs.

Comparison of stress values at points 2-3 and 4-2 by FEM analysis and those recorded in the load test，as shown in Fig. 10. It can be seen that: The trend of the stress response curve measured by the real bridge test is consistent with the FEM results. The measured data is reliable. The local effect of stress distribution is remarkable.

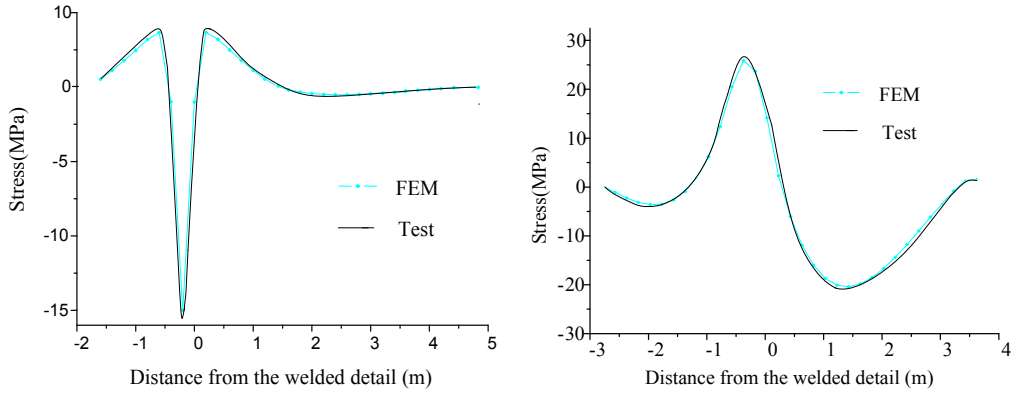


(a) Measuring point 2-3 (b) Measuring point 4-2

**Figure 10:** Comparison of stress values by FEM analysis and those recorded in the load test

## 4 Fatigue cumulative damage calculation method for welded details

### *4.1 Palmgren-Miner linear cumulative damage theory*

Palmgren-Miner linear damage accumulation theory is been widely used to evaluate the fatigue life of the bridge based on the existing amplitude and constant amplitude data, which states that the total fatigue damage is a linear superposition of fatigue damage caused by different variable amplitude stress cycles. The total fatigue damage is:

$$D=\sum_{i=1}^{n}\frac{n_i}{N_i}=\frac{n_1}{N_1}+\frac{n_2}{N_2}+\frac{n_3}{N_3}\cdots+\frac{n_n}{N_n} \tag{1}$$

$$L=\frac{1}{D}=\frac{1}{\sum_{i=1}^{n}\frac{n_i}{N_i}} \tag{2}$$

In the formula: $D$ is the total fatigue damage, $L$ is the structural fatigue life, $n_i$ is the number of cycles generated by the variable amplitude stress cycle $S_i, N_i$ is the fatigue life corresponding to stress cycle $S_i$ in constant $S-N$, $i$ is the number of stress amplitude levels. Miner's linear cumulative damage criterion assumes that at $D \geq 1$, fatigue failure.

### *4.2 The S-N curve of Eurocode3*

According to the *S-N* curve, the fatigue life of the material can be determined. For variable amplitude fatigue, when all stress cycles are greater than the constant fatigue limit CAFL (Constant Amplitude Fatigue Limit), the fatigue life of the structure can be accurately calculated according to the Miner criterion and the *S-N* curve; when the stress cycle number is smaller than CAFL, the structural life is considered to be infinite and the effect of the low stress cycle is not considered. However, there are generally both high stress cycles larger than CAFL and low stress cycles smaller than CAFL in bridges. In order to accurately calculate the fatigue life of the structure, the fatigue damage caused by the low stress cycle should be properly dealt with in the fatigue strength curve.

In the *S-N* curve of Eurocode3 [EC3 (2004)], not only the stress state of the welded details in the orthotropic steel bridge deck is considered, but also the low-level stress cycle that is less than the constant fatigue limit CAFL is considered. In addition, for the classification of fatigue details, British BS5400 specification and China TB99 have not given specific classification of welded details in orthotropic steel decks. The detailed classification in the American specification is not comprehensive. The classification of welded details for closed orthotropic steel decks are given in detail in the Eurocode3 specification. The $S-N$ curve in Eurocode3 specification is shown in Fig. 11.

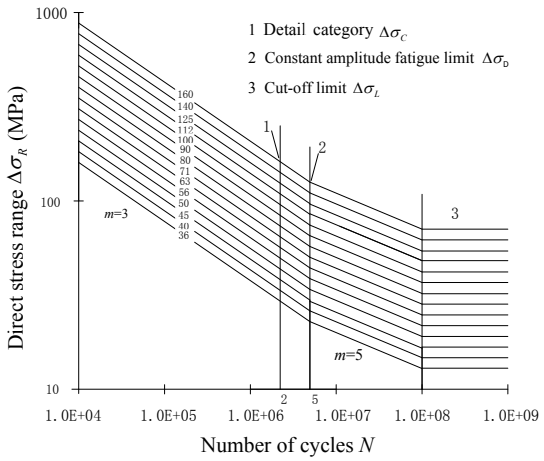


**Figure 11:** Fatigue strength curves for direct stress ranges (Eurcode 3, 2004)

Eurocode3 states that the extended fatigue strength curve is:

$$\Delta\sigma_R^m N_R = \Delta\sigma_C^m \cdot 2\times10^6 \qquad m=3, \quad N \leq 5\times10^6 \tag{3}$$

$$\Delta\sigma_R^m N_R = \Delta\sigma_D^m \cdot 5\times10^6 \qquad m=5, \quad 5\times10^6 \le N \le 10^8 \tag{4}$$

Here: $\Delta\sigma_R$ is the stress range of welded details. $N_R$ is the fatigue life. $\Delta\sigma_D$ is the constant amplitude fatigue limit for each welded detail. When the stress range $S$ is greater than $\Delta\sigma_D$, the fatigue strength coefficient is $K_C$. When the stress range $S$ is less than $\Delta\sigma_D$, the fatigue strength coefficient is $K_D$.

In addition, the specification also determines the stress cutoff limit when the number of cycles is $10^8$:

$$\Delta\sigma_L = \left(\frac{5}{100}\right)^{1/5} \cdot \Delta\sigma_D = 0.549\Delta\sigma_D \tag{5}$$

When $\Delta\sigma_R \le \Delta\sigma_L$, it is assumed that the stress cycle does not cause fatigue damage. Therefore, $\Delta\sigma_L$ can also be regarded as the variable amplitude fatigue limit (VAFL) [Deng, Li and Ding (2014)].

The classification of welded details can be obtained From Eurocode3 Part1-9. According to formula (5) and formula (6), each fatigue strength curve parameter of welded details can be calculated, as shown in Tab. 2.

**Table 2:** Fatigue strength curve parameter of welded details (MPa)

| Welded details | Detail category | Constant amplitude fatigue limit | Cut-off limit |
|---|---|---|---|
| Deck plate-to-rib | 71 | 52 | 29 |
| U-rib butt joint | 50 | 37 | 20 |
| Diaphragm plate opening | 71 | 52 | 29 |
| Deck plate-to-rib-to-diaphragm | 80 | 59 | 32 |

### *4.3 Fatigue cumulative damage calculation method*

The fatigue failure of the structure is mainly manifested as crack propagation. In the detailed weld, there are inevitably small cracks or defects. Under the repeated action of the high stress cycle, cracks will be generated and continue to expand. The low stress cycle before the cracks can be neglected, but after cracks appear, low stress cycles promote crack propagation and cause damage. Therefore, it is unreasonable to ignore the effect of low stress range when calculating the detail fatigue life. When the high stress range is present, the so-called "fatigue threshold" concept [Chan, Li and Ko (2001)] is not fully applicable and all stress cycles should be considered. In order to obtain accurate welding details of fatigue life, this paper takes into account the fatigue damage caused by the stress cycle below the cutoff limit $\Delta\sigma_L$ in the *S-N* curve and counts it into $S \le \Delta\sigma_D$. According to fatigue damage equivalence principle and the Eurocode3 specification (Eurocode3, 2014), the formula for the equivalent stress range $S_{eq}$ [Deng, Li and Ding (2014)] is

$$S_{eq} = \left[ \frac{\sum_{S_{i\geq\Delta\sigma_D}} \frac{n_i S_i^3}{K_C} + \sum_{S_{j\leq\Delta\sigma_D}} \frac{n_j S_j^5}{K_D}}{N_d / K_D} \right]^{\frac{1}{5}} \tag{6}$$

$$N_d = \sum_{S_{i\geq\Delta\sigma_D}} n_i + \sum_{S_{i\leq\Delta\sigma D}} n_j \tag{7}$$

Based on the Miner criterion, the formula for calculating the fatigue life of each detail can be obtained:

$$L = \frac{1}{D} = \frac{1}{\sum_{S_i \geq \Delta\sigma_D} \frac{n_i S_i^3}{K_C} + \sum_{Sj<\Delta\sigma_D} \frac{n_j S_j^5}{K_D}} \tag{8}$$

In the formula: $S_i$ is the stress cycle greater than or equal to $\Delta\sigma_D$, $S_j$ is the stress cycle less than $\Delta\sigma_D$, $n_i$, $n_j$ are the numbers of action cycles greater than or equal to $\Delta\sigma_D$ and less than $\Delta\sigma_D$, respectively.

## 5 Fatigue life evaluation of welded details

### *5.1 Test results*

For the measured strain-time curve by the test, the fatigue stress spectrum of each measuring point is obtained through the simplified rain flow counting method [AASHTO LRFD (2005)], and the numbers of stress ranges cycles at each level is obtained. Sections 3 and 4 include the typical details. Due to space limitations, only the stress spectra and stress cycle numbers for each of Sections 3 and 4 are given.

Fig. 12 shows the stress spectra at each measuring point of Section 3. Cross section 3 is at the position of the diaphragm. Mainly measured stresses of deck-to-rib welds, U rib butt joint, U-rib-to-diaphragm welds, and the diaphragm openings. In Figs. 7(a), 7(b) is a 14 mm thick deck-U rib welds stresses, (e), (f) are the stresses of the diaphragm openings welded detail and U-rib-to-diaphragm welds; (c), (d), and (g) in the drawings are the weld positions corresponding to (a), (b), and (e) when the top plate thickness is 16 mm.

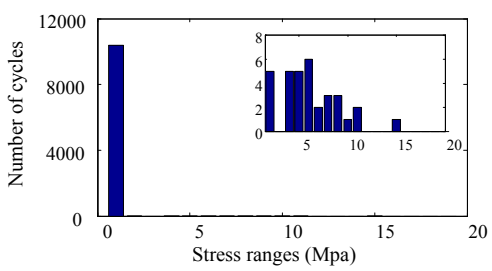


(a) 3-1/3-2

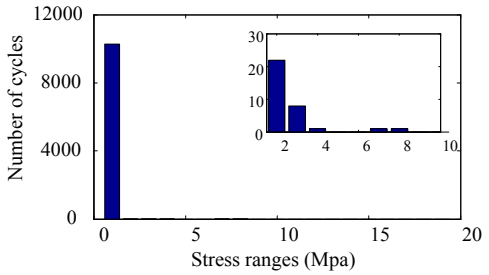


(b) 3-3/3-4

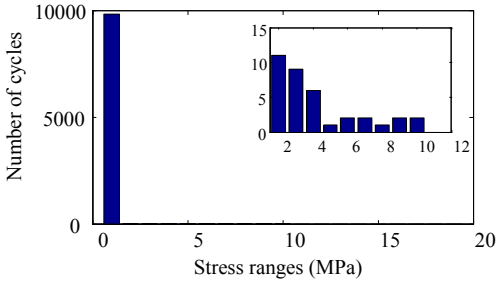


(c) 3-5/3-6

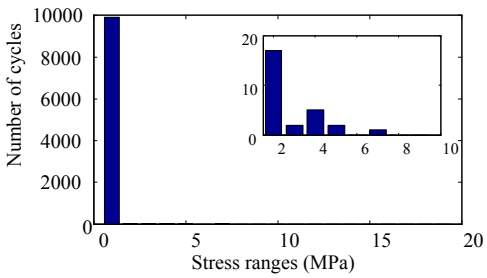


(d) 3-7/3-8

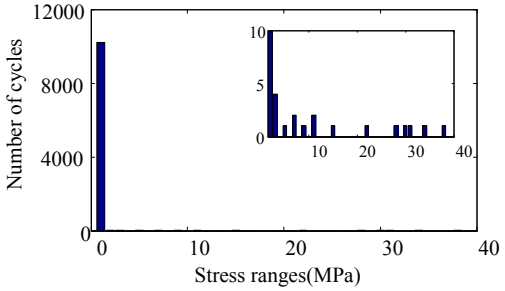


(e) 3-9/3-10/3-11

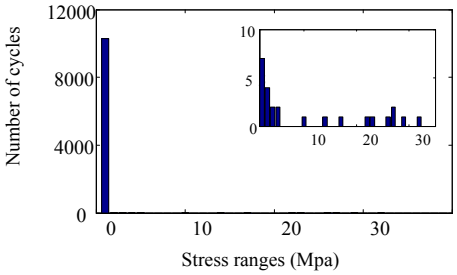


(f) 3-12/3-13/3-14

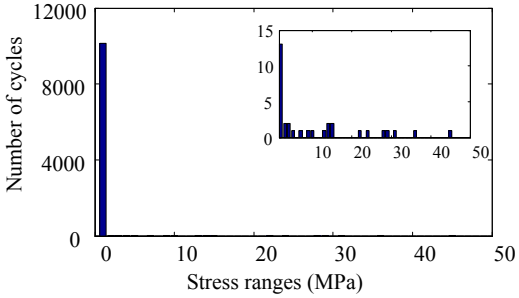


(g) 3-15/3-16/3-17

**Figure 12:** Stress spectra on Section 3

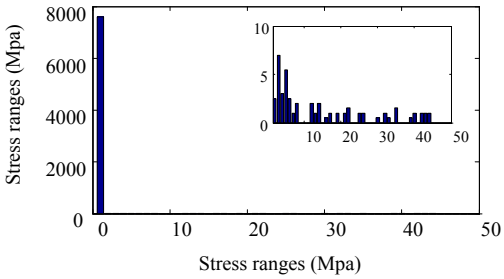


(a) 4-1

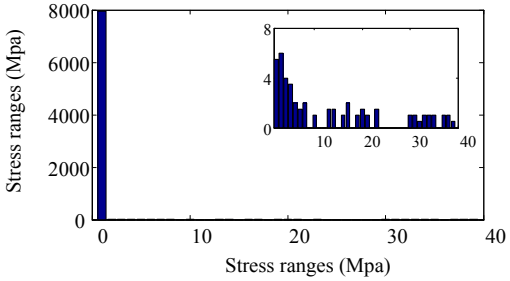


(b) 4-2

**Figure 13:** Stress spectra on Section 4

Fig. 13 shows the stress spectra at each measuring point on Section 4. Section 4 mainly measures the stress of the U-rib butt joint. Measuring point 4-1 is at the position of the 14 mm thick deck plate, and measuring point 4-2 is at the position of the 16 mm thick deck plate.

It can be seen from Figs. 12 and 13 that there are many stress cycles with very small stress ranges, which basically reach $10^4$ orders of magnitude. The number of stress cycles at each measurement point is concentrated in the range of 0 to 1 MPa. Since a large number of small stresses contain a large number of random disturbance signals, the fatigue stress range of 0 to 1 MPa can be directly ignored in the fatigue damage calculation of each weld. At the same time, studies have shown [Deng, Ding and Li (2013)] that discarding a stress cycle of less than 2 MPa has little effect on the calculation of fatigue life. Therefore, only the stress range greater than or equal to 2 MPa is considered in the fatigue life calculation in this paper.

Tab. 3 lists the number of stress cycles corresponding to the different stress ranges of Sections 3 and 4 measured by the rain-flow counting method. The numbers of cycles of the stress range of the weld from the position of each section measuring point can be found:

① On Section 3, the stress ranges of the deck plate-to-rib welds are mainly distributed in the range of 2 to 10 MPa, indicating that the deck plateto-rib welds in Sections 3 at most experience low-amplitude stress cycles.

② On Section 4, the stress range of U-rib butt joint is larger and is distributed in the range of 2 to 46 MPa.

Tab. 3, Tab. 4 and Tab. 5 list the stress cycle numbers corresponding to the different stress ranges of Sections 1-5 measured by the rain-flow counting method. The cycle numbers of the stress ranges of the weld from the position of each section measuring point can be found:

① The stress ranges of the deck plate-to- rib welds are mainly distributed in the range of 2 to 10 MPa, indicating that the deck-U ribs welding detail most experience low-amplitude stress cycles.

② the U rib butt weld has a large stress amplitude and is distributed in the range of 2 to 46 MPa.

**Table 3:** Number of cycles on Sections 1 and 2 measuring points

| Stress ranges (MPa) | Deck plate thickness on Section 1 (mm) | | | | Stress ranges (MPa) | Deck plate thickness on Section 2 (mm) | | | |
|---|---|---|---|---|---|---|---|---|---|
| | 14 | | 16 | | | 14 | | 16 | |
| | 1-1/1-2 | 1-3/1-4 | 1-5/1-6 | 1-7/1-8 | | 2-1 | 2-2 | 2-3 | 2-4 |
| 1 | 1-5/1-6 | 1-7/1-8 | 3105 | 5290 | 1 | 3216.5 | 3417 | 2988 | 4319.5 |
| 2 | 5717.5 | 5799 | 3 | 14 | 2 | 13 | 6.5 | 13 | 5 |
| 3 | 14 | 23 | 7 | 6 | 3 | 6 | 3 | 8 | 7 |
| 4 | 6 | 6 | 2 | 5 | 4 | 11 | 5 | 6 | 3 |
| 5 | 5 | | 4 | 2 | 5 | 7.5 | 4 | 3 | 2 |
| 6 | 3 | | 2 | | 6 | 8 | 1 | 3.5 | |
| 7 | 4 | | | | 7 | | | 3 | 2 |

| | | | | | | | | | |
|---|---|---|---|---|---|---|---|---|---|
| 8 | 2 | | | | 8 | 1.5 | 1 | 2 | 2 |
| 9 | 2 | 1 | 1 | 1 | 9 | 4 | 2 | 3.5 | 1 |
| 10 | 3 | 1 | 1 | | 10 | | | | 1 |
| 11 | | | | | 11 | 2 | 4 | 1 | 3 |
| 12 | | 1 | 2 | | 12 | 0.5 | | 1 | 1 |
| 13 | | | | | 13 | | 2.5 | 0.5 | 1.5 |
| 14 | | | 2 | | 14 | 1 | 1 | 1 | 0.5 |
| 15 | | | 1 | | 15 | | | | 0.5 |
| 16 | | | 1 | | 16 | 0.5 | 0.5 | | 0.5 |
| | | | | | 17 | 1.5 | 0.5 | 1 | |
| | | | | | 18 | | | 0.5 | |
| | | | | | 19 | | 0.5 | | |
| | | | | | 20 | 0.5 | | | |
| | | | | | 21 | 0.5 | | | |
| | | | | | 25 | 0.5 | | | |

**Table 4:** Number of cycles on Sections 3 and 4 measuring points

| Stress ranges (MPa) | Deck thickness on Section 3 (mm) | | | | | | | Stress ranges (MPa) | Deck thickness on Section 3 (mm) | |
|---|---|---|---|---|---|---|---|---|---|---|
| | 14 | | | | 16 | | | | 14 | 16 |
| | 3-1/3-2 | 3-3/3-4 | 3-9/10/11 | 3-12/13/14 | 3-5/3-6 | 3-7/3-8 | 3-15/16/17 | | 4-1 | 4-2 |
| 1 | 10377 | 10266.5 | 10135.5 | 10272 | 9851.5 | 9916.5 | 10212 | 1 | 7592.5 | 7955.5 |
| 2 | 5 | 22 | 13 | 7 | 11 | 17 | 10 | 2 | 2.5 | 5.5 |
| 3 | | 8 | 2 | 4 | 9 | 2 | 4 | 3 | 7 | 6 |
| 4 | 5 | 1 | 2 | 2 | 6 | 5 | | 4 | 3 | 4 |
| 5 | 5 | | 1 | 2 | 1 | 2 | 1 | 5 | 5.5 | 3.5 |
| 6 | 6 | | | | 2 | | | 6 | 2.5 | 2 |
| 7 | 2 | 1 | 1 | | 2 | 1 | 2 | 7 | 1 | 1.5 |
| 8 | 3 | 1 | | | 1 | | | 8 | 2 | 2 |
| 9 | 3 | | 1 | | 2 | | 1 | 10 | | 1 |
| 10 | 1 | | 1 | 1 | 2 | | | 12 | 2 | |
| 11 | 2 | | | | | | 2 | 13 | 1 | 1.5 |
| 12 | | | | | | | | 14 | 2 | 1.5 |
| 13 | | | 1 | | | | | 16 | 0.5 | 1 |
| 14 | | | 2 | 1 | | | | 17 | 1 | 2 |
| 15 | | | 2 | | | | 1 | 19 | 1 | 1 |
| 17 | | | | | | | | 20 | | 1.5 |
| 18 | | | | 1 | | | | 21 | 1 | 1 |
| 22 | | | 1 | 1 | | | 1 | 22 | 1.5 | |
| 23 | | | | 1 | | | | 23 | | 1.5 |

| | | | | | | |
|---|---|---|---|---|---|---|
| 24 | 1 | | | 25 | 1 | |
| 26 | | 1 | | 26 | 1 | |
| 27 | | 2 | | 30 | 0.5 | 1 |
| 28 | 1 | | 1 | 31 | | 1 |
| 29 | 1 | 1 | | 32 | 1 | 0.5 |
| 30 | | | 1 | 33 | 0.5 | 1 |
| 31 | 1 | | 1 | 34 | | 1 |
| 32 | | 1 | | 35 | 1.5 | 1 |
| 34 | | | 1 | 37 | | 1 |
| 36 | 1 | | | 38 | | 1 |
| 38 | | | 1 | 39 | 0.5 | 0.5 |
| 47 | 1 | | | 40 | 1 | |
| | | | | 42 | 1 | |
| | | | | 43 | 1 | |
| | | | | 46 | 1 | |

**Table 5:** Number of cycles on Section 5 measuring points

| Stress ranges (MPa) | Deck thickness on Section 3 (mm) | | | |
|---|---|---|---|---|
| | 14 | | 16 | |
| | 5-1/5-2 | 5-3/5-4 | 5-5/5-6 | 5-7/5-8 |
| 1 | 9830.5 | 8165.5 | 9881.5 | 9765 |
| 2 | 3 | 10.5 | 2 | 2 |
| 3 | 7 | 5 | 3 | 3 |
| 4 | 3 | 2 | 1 | 5 |
| 5 | 3 | 3 | 3 | 2 |
| 6 | 4 | 2 | 1 | 3 |
| 7 | 3 | 1 | 5 | |
| 8 | 4 | 2 | 2 | 2 |
| 9 | 2 | 1.5 | 2 | |
| 10 | 2 | 0.5 | 3 | 1 |
| 11 | | | 2 | 1 |
| 12 | | | 2 | 2 |
| 13 | 1 | | | |
| 15 | | | | 4 |
| 16 | | | 1 | |
| 17 | | | 1 | 2 |
| 18 | | | 1 | |
| 20 | | | 1 | 1 |
| 28 | | | 1 | |

### *5.2 Fatigue life of welded details*

From the cut-off limit $\Delta\sigma_L$ value of the welding details in Tab. 1, the stress amplitudes of the measured welding details at different measuring points of each monitoring section can be judged. Both the stress amplitude greater than the deadline and the stress amplitude less than the deadline. The stress amplitude less than $\Delta\sigma_L$ is included in the fatigue damage calculation and is classified in the range of the formula (7) which is smaller than the constant fatigue limit $\Delta\sigma_D$. Formula (8) and Formula (9) are available as following:

(1) Deck plate-to- rib welded details and diaphragm openings:

$$K_C = \Delta\sigma_C^3 \cdot 2\times10^6 = 2.50\times10^{11}$$

$$K_D = \Delta\sigma_D^3 \cdot 5\times10^6 = 3.47\times10^{14}$$

(2) U-rib but joints:

$$K_C = \Delta\sigma_C^3 \cdot 2\times10^6 = 7.16\times10^{11}$$

$$K_D = \Delta\sigma_D^3 \cdot 5\times10^6 = 1.90\times10^{15}$$

(3) Deck plate-to- rib-to-diaphragm:

$$K_C = \Delta\sigma_C^3 \cdot 2\times10^6 = 1.02\times10^{12}$$

$$K_D = \Delta\sigma_D^3 \cdot 5\times10^6 = 3.57\times10^{15}$$

The fatigue life of each detail is calculated from Eq. (7), as shown in Tab. 6.

It can be seen from Tab. 6:

(1) U-rib butt joints and the diaphragm opening welded details are susceptible to fatigue failure. Among them, the fatigue life of the U-butt weld of position 1 (14 mm top plate thickness) is the shortest, followed by position 2 (16 mm top plate thickness). The fatigue life of the openings of the diaphragms at positions 1 and 2 is comparable;

(2) From the fatigue life of the cross-sections of Section 3 and Section 5, it can be seen that for the deck plate-to-rib welded details. The fatigue life of the detail using the diaphragm is significantly longer than that without the diaphragm. This shows that the arrangement of the diaphragm can enhance the fatigue performance of the welded joints between the top plate and the U-ribs, and improve their fatigue life.

(3) For each section, the fatigue life of the measured points at Location 2 is greater than that at the corresponding measured at Location 1, which can be used to predict that the U-rib butt weld at Location 1 will experience the first fatigue failure. It is advisable to pay special attention to the damage of the U-rib butt and the weld at the opening of the diaphragm during the operation of the bridge and carry out timely fatigue tests.

**Table 6:** Fatigue life of welded details

| Sections | Deck thickness (mm) | Measuring point location | Welding Detail types | Fatigue life |
|---|---|---|---|---|
| Section 1 | 14 | 1-1/1-2 | Deck plate-to-rib | 1071642547 |
| | | 1-3/1-4 | Deck plate-to-rib | 1360453537 |
| | 16 | 1-5/1-6 | Deck plate-to-rib | 1971387733 |
| | | 1-7/1-8 | Deck plate-to-rib | 4797787764 |
| Section 2 | 14 | 2-1 | Deck plate-to-rib | 183330018 |
| | | 2-2 | Deck plate-to-rib | 123410797 |
| | 16 | 2-3 | Deck plate-to-rib | 231167355 |
| | | 2-4 | Deck plate-to-rib | 127050660 |
| Section 3 | 14 | 3-1/3-2 | Deck plate-to-rib | 728034140 |
| | | 3-3/3-4 | Deck plate-to-rib | 6516799068 |
| | | 3-9/10/11 | diaphragm plate opening | 9446049 |
| | | 3-12/13/14 | Deck plate-to-rib-to-Diaphragm | 32821058 |
| | 16 | 3-5/3-6 | Deck plate-to-rib | 842560218 |
| | | 3-7/3-8 | Deck-U-rib | 11880713528 |
| | | 3-15/16/17 | diaphragm plate opening | 9585804 |
| Section 4 | 14 | 4-1 | U-rib butt joint | 2330774 |
| | 16 | 4-2 | U-rib butt joint | 4449858 |
| Section 5 | 14 | 5-1/5-2 | Deck plate-to-rib | 13257040 |
| | | 5-3/5-4 | Deck plate-to-rib | 34920151 |
| | 16 | 5-5/5-6 | Deck plate-to-rib | 378725039 |
| | | 5-7/5-8 | Deck plate-to-rib | 1391102158 |

## 6 Conclusions

According to the measured strain data of the steel box girder test of Taizhou Bridge, this paper studies the fatigue life of welded details of flat steel box girders based on Miner linear cumulative damage theory. The following conclusions can be drawn:

(1) The local effect of stress distribution is remarkable. The stress values obtained from the load test is consistent with the FEM result, indicating that the data measured by the load test is reliable.

(2) The stress measured points are mainly based on low-amplitude stress cycles, and most of the stress amplitudes are in the range of 2 to 10 MPa, the welding details stress at the U-rib butt joint is larger among the stress amplitudes.

(3) The fatigue life of each welded detail at 14 mm thick deck plate position is smaller than that at at 16 mm thick deck corresponding to the fatigue life of the weld.

(4) U-rib butt joints, openings in the diaphragm is easy to fatigue damaged. Among them, the 14 mm thick U-rib butt joints first appeared fatigue failure.

(5) The arrangement of the diaphragm can effectively increase the fatigue life of the top-U rib weld and improve the fatigue performance at this detail.

**Acknowledgement:** This study was financially supported by the National Natural Science Foundation, China (51778135), the Natural Science Foundation of Jiangsu Province, China (BK20160207), Aeronautical Science Foundation, China (20130969010), the Fundamental Research Funds for the Central Universities and Postgraduate Research & Practice Innovation Program of Jiangsu Province, China (KYCX18_0113; KYLX16_0253) and the National Key Research and Development Program of China (2017YFC0806001).

**References**

**AASHTO** (2010): *AASHTO Bridge Element Inspection Guide Manual*. AASHTO, Washington, D.C.

**AASHTO** (2012): *AASHTO LRFD Bridge Design Specifications*. AASHTO, Washington, D.C.

**AISC** (2010): *Hollow Structural Sections Connections Man*ual, AISC, Chicago.

**BS5400** (1980): *Steel, Concre and Composite Bridge-Part10: Code of Practice for Fatigue.* BSI, London.

**Chang, K. O.; Bae, D.** (2014): Proposed revisions to fatigue provisions of orthotropic steel deck systems for long span cable bridges. *International Journal of Steel Structures*, vol. 14, no. 4, pp. 811-819.

**Chan, T. H. T.; Li, Z. X.; Ko, J. M.** (2001): Fatigue analysis and life prediction of bridges with structural health monitoring data-Part II: application. *International Journal of Fatigue*, vol. 23, no. 1, pp. 55-64.

**Deng, Y.; Ding, Y. L.; Li, A. Q.** (2013): Fatigue reliability assessment for welded details of steel box girders using long-term monitoring data: fatigue reliability indicies. *China Civil Engineering Journal*, vol. 45, no. 3, pp. 86-92.

**Deng, Y.; Li, A. Q.; Ding, Y. L.** (2014): Analysis of monitoring mass strain data and fatigue assessment for steel-box-girder bridges. *Engineering mechanics*, vol. 31, no. 7, pp. 69-77.

**EC3** (2004): *Eurocode3: Design of Steel Structures-Part 1.9: Fatigue.* ECS.

**Fisher, J. W.; Roy, S.** (2011): Fatigue of steel bridge infrastructure. *Structure & Infrastructure Engineering*, vol. 7, no. 7-8, pp. 457-475.

**Fu, Z.; Ji, B.; Zhang, C.; Wang, Q.** (2017). Fatigue performance of roof and u-rib weld of orthotropic steel bridge deck with different penetration rates. *Journal of Bridge Engineering*, vol. 22, no. 6, 04017016.

**Gurney, T.** (2006): *Cumulative Damage of Welded Joints*. CRC Press.

**Guo, T.; Chen, Y. W.** (2013): Fatigue reliability analysis of steel bridge details based on field-monitored data and linear elastic fracture mechanics. *Structure & Infrastructure Engineering*, vol. 9, no. 5, pp. 496-505.

**Ju, X.; Tateishi, K.** (2014). Fatigue crack behavior at rib-to-deck weld bead in orthotropic steel deck. *Advances in Structural Engineering*, vol. 17, no. 10, pp. 1459-1468.

**Ji, B.; Liu, R.; Chen, C.; Maeno, H.; Chen, X.** (2013). Evaluation on root-deck fatigue of orthotropic steel bridge deck. *Journal of Constructional Steel Research*, vol. 90, no. 5, pp. 174-183.

**Kozy, B. M.; Connor, R. J.** (2010). Fatigue design of orthotropic steel bridges. *Structures Congress*, pp. 541-553.

**Liu, Y.; Xiao, X.; Lu, N.; Deng, Y.** (2016): Fatigue reliability assessment of orthotropic bridge decks under stochastic truck loading. *Shock and Vibration*, vol. 2016, no. 3, pp. 1-10.

**Liu, Y. M.; Zhang, Q. H.; Zhang, P.; Cui, C.** (2016): Study on fatigue life of u-rib butt weld in orthotropic steel bridge deck of Hong Kong-Zhuhai-Macao bridge. *China Journal of Highway & Transport*, vol. 29, no. 12, pp. 25-33.

**Miao, C. Q.; Shi, C. H.** (2013). Temperature gradient and its effect on flat steel box girder of long-span suspension bridge. *Science in China-Series E: Technological Sciences*, vol. 56, no. 8, pp. 1929-1939.

**Sim, H. B.; Uang, C. M.** (2012). Stress analyses and parametric study on full-scale fatigue tests of rib-to-deck welded joints in steel orthotropic decks. *Journal of Bridge Engineering*, vol. 17, no. 5, pp. 765-773.

**Song, Y. S.; Ding, Y. L.; Wang, X. J.; Li, A. Q.** (2013): Monitoring and analysis of fatigue effects on steel deck of a suspension bridge in working conditions. *Engineering mechanics*, vol. 30, no. 11, pp. 94-100.

**Tang, L.; Huang, L.; Liu, G.; Wang, C.; Fu, B.** (2014): Fatigue experimental study of a full-scale steel orthotropic deck model. *China Civil Engineering Journal*, vol. 47, no. 3, pp. 112-122.

**Yang, S. L.; Zhou, S.** (2017): Current research of fatigue damage in orthotropic deck plates of long span steel box girder bridges in China. *Bridge Construction*, vol. 47, no. 4, pp. 60-65.

**Ya, S.; Yamada, K.; Shikawa, T.** (2011): Fatigue evaluation of rib-to-deck welded joints of orthotropic steel bridge deck. *Journal of Bridge Engineering*, vol. 18, no. 5, pp. 492-499.

**Zeng, Z. B.** (2011): Classification and reasons of typical fatigue cracks in orthotropic steel deck. *Steel Construction*, vol. 26, no. 2, pp. 9-15, 26.

**Zhang, Q.; Cui, C.; Bu, Y.; Li, Q.** (2014): Study on fatigue features of orthotropic decks in steel box girder of Hong Kong-Zhuhai-Macao Bridge. *China Civil Engineering Journal*, vol. 47, no. 9, pp. 110-119.

**Zhang, Q. H.; Cui, C.; Bu, Y. Z.; Liu, Y. M.; Ye, H. W.** (2015): Fatigue tests and fatigue assessment approaches for rib-to-diaphragm in steel orthotropic decks. *Journal of Constructional Steel Research*, vol. 114, pp. 110-118.

**Zhang, Q. H.; Bu Y. Z.; Qiao, L. I.** (2017): Review on fatigue problems of orthotropic steel bridge deck. *China Journal of Highway & Transport*, vol. 30, no. 3, pp. 14-30, 39.

**Zhu, A.; Li, M.; Tian, Y.; Xiao, H.; He, D. et al.** (2017): Fatigue test on full-scale orthotropic steel bridge deck with inner diaphragm. *Steel Construction*, vol. 32, no. 217, pp. 45-50.